

# In-orbit performance of the EPIC-MOS detectors on XMM-Newton

S. Sembay<sup>a</sup>, A. Abbey<sup>a</sup>, B. Altieri<sup>b</sup>, R. Ambrosi<sup>a</sup>, D. Baskill<sup>a</sup>, P. Ferrando<sup>c</sup>, K. Mukerjee<sup>a</sup>,  
A. Read<sup>a</sup> and M. J. L. Tumer<sup>a</sup>

<sup>a</sup>Department of Physics, Leicester University, UK;

<sup>b</sup>XMM-SOC, ESA/Vilspa, Spain;

<sup>c</sup>CEA/Sap, Saclay, France

## ABSTRACT

XMM-Newton was launched into space on a highly eccentric 48 hour orbit on December 10th 1999. XMM-Newton is now in its fifth year of operation and has been an outstanding success, observing the Cosmos with imaging, spectroscopy and timing capabilities in the X-ray and optical wavebands. The EPIC-MOS CCD X-ray detectors comprise two out of three of the focal plane instruments on XMM-Newton. In this paper we discuss key aspects of the current status and performance history of the charge transfer inefficiency (CTI), energy resolution and spectral redistribution function (rmf) of EPIC-MOS in its fifth year of operation.

Keywords: XMM-Newton, EPIC-MOS CCD, X-ray detectors, Radiation Damage

## 1. INTRODUCTION

XMM-Newton<sup>1</sup> carries three telescopes which combined provide the highest throughput of any X-ray observatory launched to date. At the focus of each telescope is a CCD-based imaging spectrometer, the trio making up the European Photon Imaging Camera (EPIC). Two of the cameras (EPIC-MOS) use seven EEV type 22 MOS CCDs<sup>2</sup> each whilst the third (EPIC-pn) uses twelve pn CCDs.<sup>3</sup>

The design of the EPIC detectors must account for the radiation environment in space in order to minimise radiation damage to the CCDs. The EPIC-MOS cameras have shielding designed to block the most damaging particles: non-relativistic protons (energies below 30 MeV) which have a high displacement cross-section. Electron divertors in each telescope prevent these particles reaching the focal plane. CTI in CCDs is temperature dependent and EPIC was designed with reserve cooling power so that the CCDs could be operated at an optimum temperature of around 120 C. Finally, the option to anneal (heat) the CCDs to repair damage is available.

## 2. THE EPIC-MOS CAMERAS IN ORBIT

### 2.1. Charge Transfer Inefficiency

Radiation damage increases the process of CTI within CCDs by displacing atoms in the silicon lattice and thereby creating sites of locally low potential. These sites are charge traps which reduce the magnitude of charge packets as they are transferred down to the readout node. The total charge lost from a given X-ray is approximately a linear function of the number of transfers from pixel to pixel. CTI also degrades the energy resolution of the CCDs because of statistical broadening. This is described in Section 2.3.

CTI is monitored by using the Fe<sub>55</sub> calibration source within the inner wheel assembly which produces strong lines at Al and Mn K. Fig. 1 shows the evolution of the CTI of the central CCDs of MOS1 and MOS2 over 800 orbits since launch.

The vertical straight lines on the plots indicate spacecraft eclipse periods and also particularly large solar ares at which discontinuities in the general increasing trend of the CTI can be detected. The upwards trend

---

Further author information: (Send correspondence to S. Sembay)

S. Sembay: E-mail: sfs5@star.le.ac.uk, Telephone: 44 116 252 3507

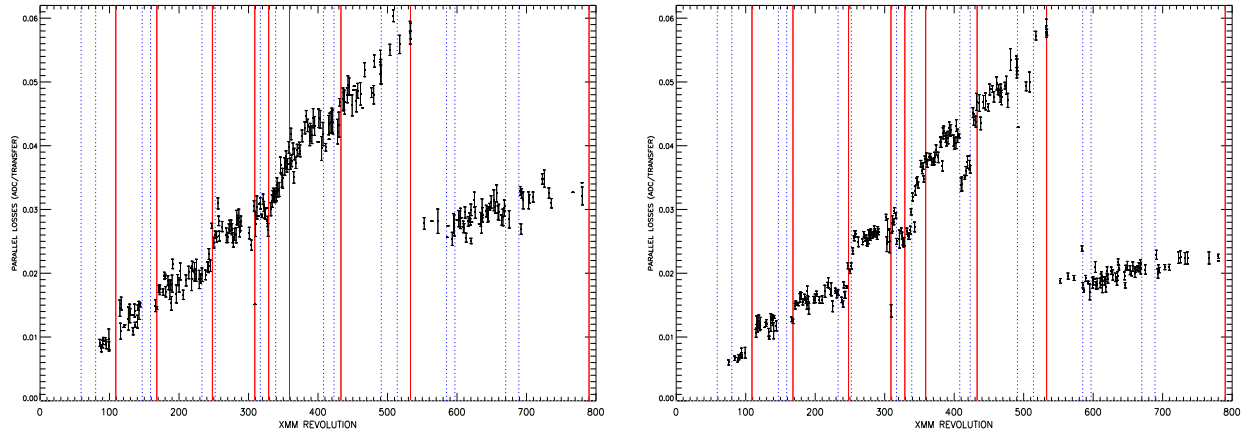


Figure 1. Parallel charge losses in units of ADC per transfer for the central CCD of MOS1 (left panel) and MOS2 (right panel) at Mn K . The gain of the CCDs are such that 1 ADC is approximately 3.25 eV. Vertical blue/dashed lines indicate spacecraft eclipse periods. Vertical red/solid lines indicate large solar flares at which discontinuities in the smoothly increasing trend in the CTI can be seen.

is consistent with pre-launch calculations of the accumulated damage due to passage of the radiation belts near perigee. The solar flares generate additional huge fluxes of high energy protons which penetrate the shielding.

The large discontinuity and partial recovery of the CTI after Orbit 534 is due to cooling of the MOS cameras from a post-launch temperature of 100 C down to 120 C. The dependence of CTI on temperature was previously demonstrated by laboratory tests carried out on an EPIC-MOS type CCD which was irradiated with  $2.5 \times 10^8 \text{ cm}^{-2} \times 10 \text{ MeV}$  equivalent protons (Fig. 2). This dosage was calculated to be typical of 5 years operation of XMM-Newton in space. Temperature affects the CTI because charge traps can be filled by electrons which allow other electrons to pass the trap safely. The electrons within the trap are released by thermal motion whose timescale is dependant on the temperature of the CCD.<sup>4</sup>

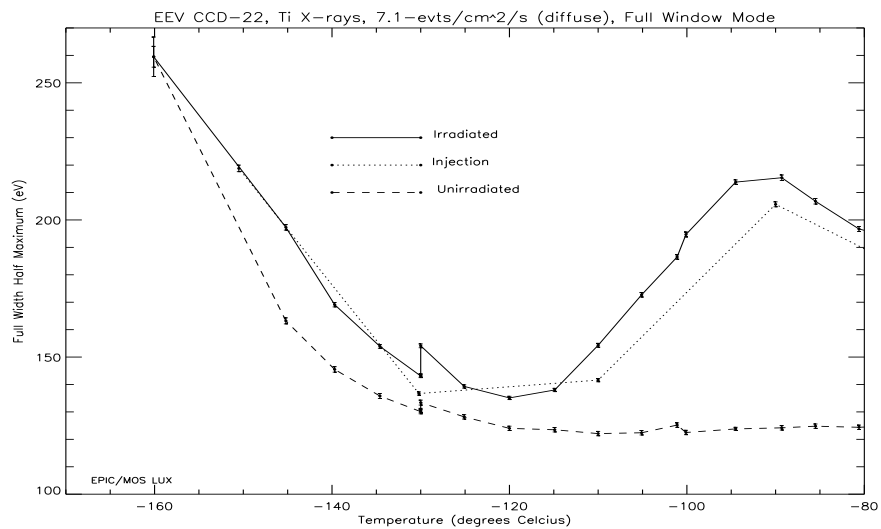


Figure 2. FWHM of the Ti K line as a function of temperature. The lowest curve is before irradiation. The top two curves are after 5 years equivalent proton irradiation with (dotted line) and without (solid line) charge injection

After some in-orbit cooling tests, described in Ferrando et al. (2003),<sup>5</sup> both cameras were cooled together during orbit 533. Observations of the isolated Neutron star RX J0720.4-3125 and the Vela Supernova Remnant taken one orbit before and after cooling demonstrated no effects on the spectral response of the CCDs apart from those arising from the improvement in CTI (Fig. 3).

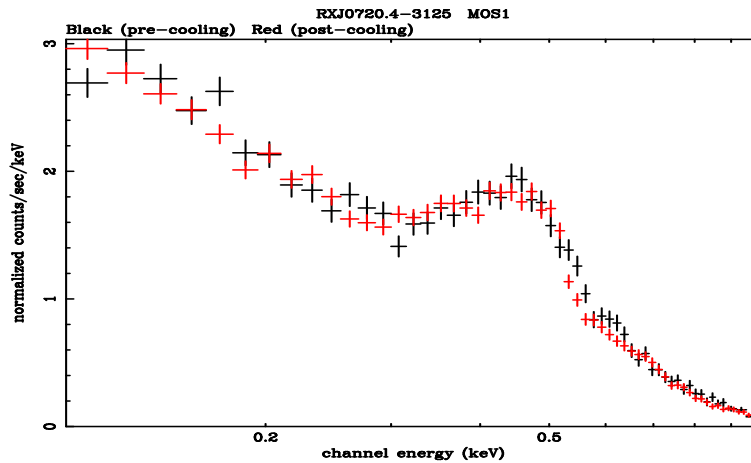


Figure 3. MOS1 spectra of the isolated NS RX J0720.4-3125 before and after cooling of the MOS CCDs. The spectra have been corrected for the pre- and post-cooling CTI losses. No significant differences are observed between the spectra.

## 2.2. Future CTI Correction

CTI shifts the observed energies of X-rays to lower energies, but can be corrected for in software in a fairly straightforward manner. The algorithm to do this has been developed collaboratively by the instrument PI team and the ESA Spacecraft Operations Centre (SOC) and is implemented within the Science Analysis System (SAS) used by observers to analyse XMM data. By design the absolute pre-launch CTI of the MOS CCDs was relatively modest<sup>6</sup> and the current CTI correction algorithm is based simply on the absolute number of transfers an event undergoes irrespective of which column(s) of the CCD the charge is deposited into.

Provision for calibrating individual columns of the CCDs was not part of the initial calibration effort. The relatively low CTI of the MOS CCDs meant that the additional computational overhead of calculating and correcting CTI for each of the 600 columns in 14 CCDs was considered prohibitively expensive. Five years is a long time in computing terms however, and the EPIC-MOS instrument team is now reinvestigating a column by column CTI correction algorithm. This should be especially beneficial to the study of line-dominated extended objects such as supernova remnants by improving the residual spatial variation in resolution and line centroid determination.

An example of the column to column variation in the line centroid at Mn K is shown in Fig. 4. The most extreme columns deviating from the average are currently masked as bad within the SAS.

## 2.3. Resolution

CTI losses are a statistical process which create an unrecoverable broadening of the energy resolution even if the best possible CTI correction algorithm were to be applied. Fig. 5 shows the evolution of the width of the CTI-corrected Mn K calibration lines on the central CCDs of MOS1 and MOS2. During eclipse periods the camera electronics are cooler and there are consequently small drops in the line width.

Since cooling the rate of degradation in resolution and CTI (Sec. 2.1) has lessened significantly. This indicates that the CCDs appear to be more robust to radiation damage at the current operating temperature of  $-120^{\circ}\text{C}$ .

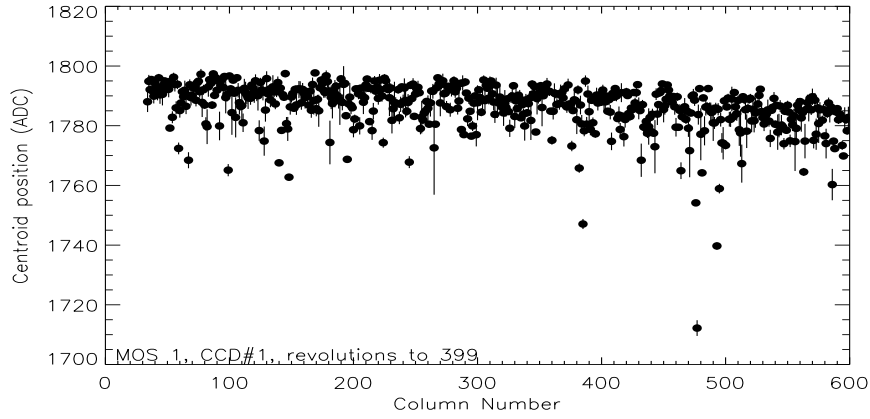


Figure 4. Mean centroid in ADC units of the uncorrected Mn K calibration line averaged over each column of the central CCD of MOS1. The data have been accumulated from closed calibration datasets summed between orbits 100 and 399. The slope in the average centroid from left to right is due to CTI in the serial register.

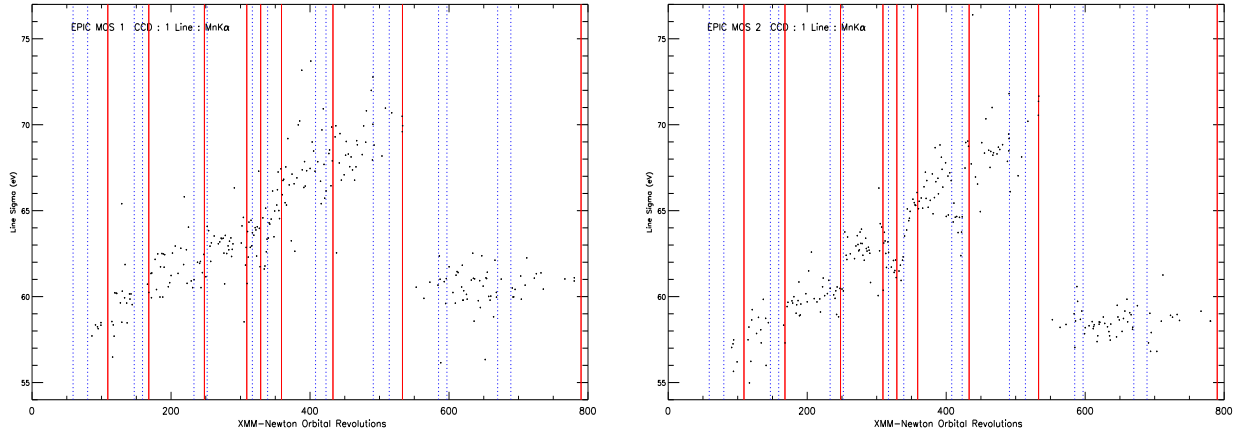


Figure 5. Evolution of the width (sigma) of the CTI-corrected Mn K line for the central CCDs of MOS1 (left panel) and MOS2 (right panel)

## 2.4. The Soft Proton Problem

The shielding designed to block high energy protons is avoided by soft protons (energies below around 300 keV) which are able to reach the CCDs because they are focussed by the grazing incidence mirrors. It was only after the launch of Chandra, a few months before XMM-Newton, that the problem of soft protons was recognised.<sup>7</sup> These protons are stopped in less than a micron of material and are potentially very damaging for front-illuminated devices such as the EPIC-MOS CCDs as shown by laboratory measurements.<sup>8</sup> In comparison the EPIC-pn is self-shielded against soft proton damage as it is a 280  $\mu$ m thick back-illuminated device.

The soft proton flux on the detectors is highly variable, varying by up to four orders of magnitude.<sup>9</sup> Flares occur most frequently during, but are not restricted to, the approach to perigee at the end of orbits. The soft protons produce background events which are nominally indistinguishable from X-rays and are not well correlated with the measured flux in the radiation monitor on XMM-Newton which is only sensitive to protons above 3.5 MeV. The original plan for protection of the cameras was for measurements taken with the radiation monitor to be used to trigger the closing of the filter wheel during periods of high radiation. This places 1.05 mm of

aluminium shielding into the field of view. The insensitivity of the radiation monitor to soft protons, however, meant that a new operational procedure was developed to use a more reliable indicator of soft proton flux to trigger the filter wheel. Good indicators such as the discarded line counter in the pn camera<sup>10</sup> and the X-ray count rate in peripheral CCDs are instrument mode dependant and are not always available throughout each orbit. It was found<sup>10</sup> that these indicators are well correlated with an RGS<sup>11</sup> parameter that records the number of events above threshold and is continuously available.

Altieri (2003)<sup>9</sup> has calculated the soft proton dosage on the cameras after 3.25 years of operations to be about  $4.6 \times 10^5$  protons  $\text{cm}^{-2}$  per EPIC-MOS camera and  $1.2 \times 10^6$  protons  $\text{cm}^{-2}$  for EPIC-pn. The difference arises because around half the proton flux is blocked by the reflection gratings within the MOS telescopes and the more stringent safety procedures for MOS which often close the cameras before pn.

The observed rate of CTI damage appears to be close to pre-launch predictions based on calculations of the high energy proton flux (Section 2.1). It would appear, therefore, that that new operational safety procedures have been quite effective in minimising the effects of soft protons in this particular regard.

## 2.5. Redistribution Function

The redistribution function (rmf) for a monochromatic input has a rather complex shape which increasingly deviates from an ideal Gaussian distribution towards lower energies. Fig. 6 shows ground calibration data taken at the Orsay synchrotron<sup>12</sup> of the central CCD of MOS1 (Flight Model Number 3) at a range of monochromatic input energies from 150 up to 440 eV. As the input energy decreases a shoulder below the main photopeak increases in relative strength until it completely dominates the rmf.

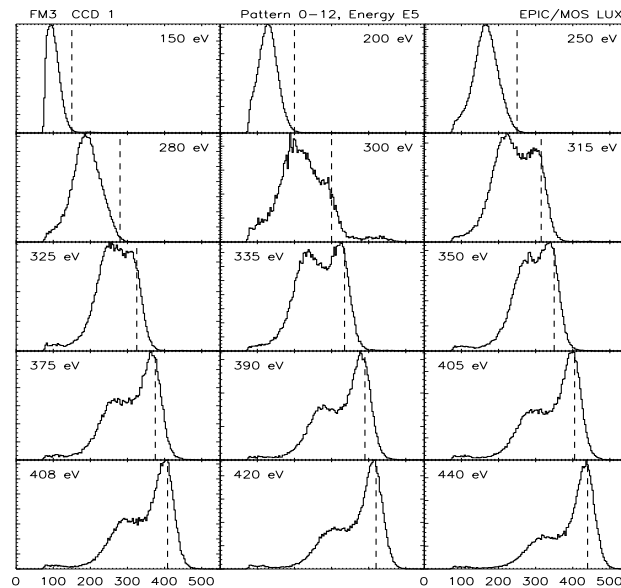


Figure 6. Ground calibration data from the central CCD of MOS1 (Flight Model 3) showing the observed spectra (after gain and CTI correction) for a series of monochromatic input energies. The evolution of the surface loss shoulder is evident.

The origin of the shoulder is thought to be incomplete charge collection for X-rays absorbed near the surface layer caused by an inversion in the surface potential.<sup>13</sup> The effect is much stronger for mono-pixels than bi-pixels (Fig. 7). The MOS CCDs have an etched open phase which was designed to increase the low energy quantum efficiency and the inversion in the surface potential is likely to be stronger in this open phase: At low energies the majority of mono-pixel events are absorbed within the open phase whereas bi-pixel events arise from photons absorbed near pixel boundaries which are partially covered by the surface electrode structure.<sup>14</sup>

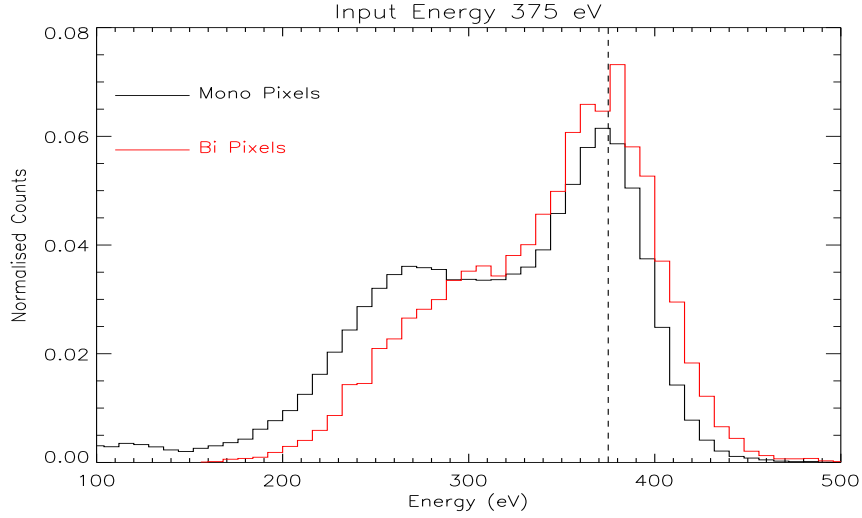


Figure 7. Ground calibration data from the central CCD of MOS1 showing normalised mono-pixel (black/bold) and bi-pixel spectra for a monochromatic beam of 375 eV. The bi-pixel spectrum has a smaller surface loss shoulder than the mono-pixel spectrum.

Analysis of astronomical targets has shown that the shape of the IMF at low energies is not constant but has evolved throughout the mission. Both cameras have been affected as illustrated by Fig. 8 which shows two sets of MOS1 spectra of the O star, *ζ* Puppis taken at different epochs, and Fig. 9 which shows MOS2 spectra of the isolated Neutron star, RX J0720.4-3125.

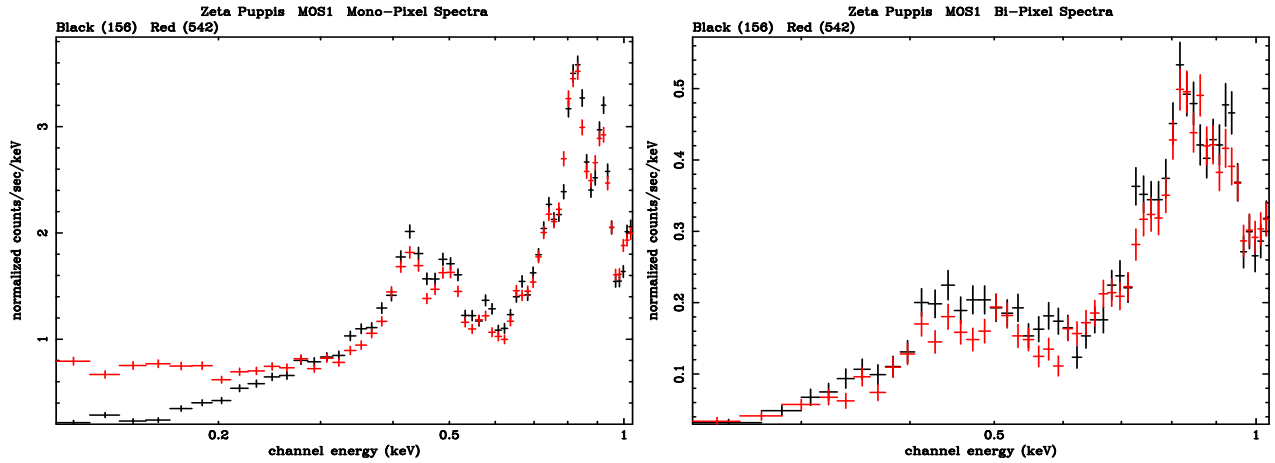


Figure 8. Mono-pixel (left panel) and bi-pixel (right panel) background subtracted spectra of the bright O star *ζ* Puppis taken in orbits 156 (black/bold) and 542.

*ζ* Puppis is an O star with strong emission lines at Nitrogen and Oxygen.<sup>15</sup> The observed flux in the MOS seen at energies below the Nitrogen lines at around 430 eV is dominated by redistribution from the lines and residual continuum at higher energies. The observations of *ζ* Puppis show a difference in the mono-pixel spectra which is not reflected in the bi-pixel spectra. Similar results are seen for MOS2. These results indicate a change in the redistribution function which must be strongest in the open phase of the CCD.

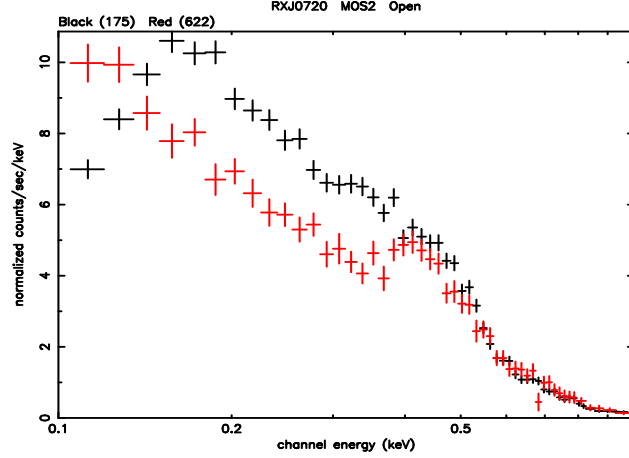


Figure 9. Mono-pixel background subtracted MOS2 spectra of the isolated neutron star, RXJ0720.4-3125, taken during orbits 175 (black/bold) and 622

The INS RXJ0720.4-3125 is now known to have a black-body like spectrum which has slightly hardened over the lifetime of XMM.<sup>16</sup> The differences in the observed MOS2 spectra (also seen in MOS1) can be attributed to a combination of this spectral evolution and a change in the rmf of the CCDs. The increase in flux below 200 eV for example must be due to an rmf change as the flux in this band is dominated by events redistributed downwards from higher energies.

The data are consistent with the degree of charge loss within the surface loss zone on the open phase increasing with time. The culprit is likely to be the soft protons which have a higher probability of reaching the active region in the open rather than the closed phase. The surface charge loss is modelled analytically by a simple linear function which describes the fractional charge loss as a function of depth within the active silicon. The parameters of the function are tuned based on the in-orbit observations of line dominated sources such as Puppis. Epoch dependant rmfs are now generated automatically by the SAS (Version 6.0 and above). Fig. 10 shows the shape of the rmf for two input energies of 300 and 425 eV appropriate for typical observations in orbits 100 and 800.

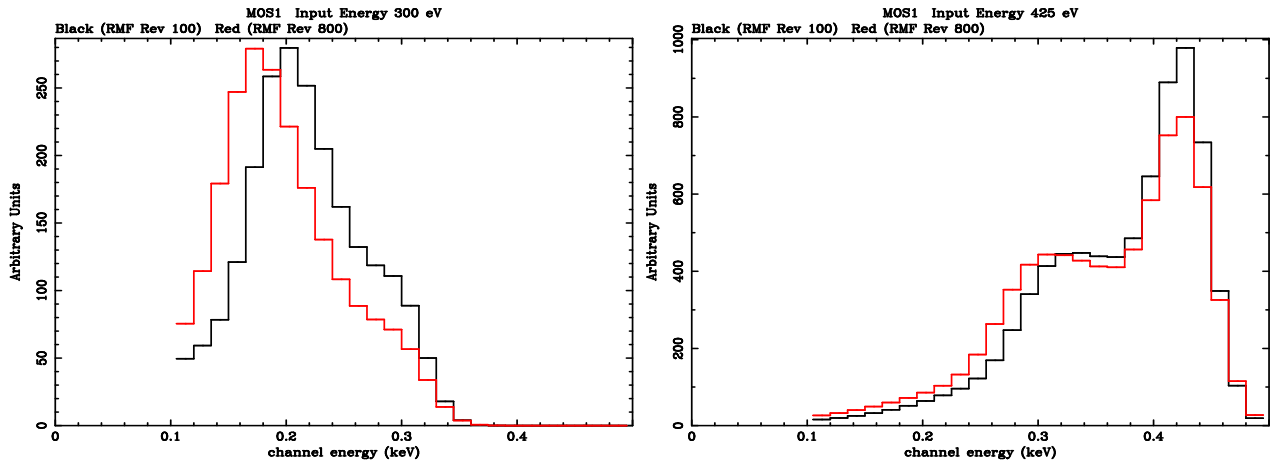


Figure 10. The shape of the MOS1 redistribution function for input energies of 300 and 425 eV. The rmfs have been generated for observations appropriate to orbits 100 (black/bold) and 800.

## ACKNOWLEDGMENTS

The authors would like to thank the many people within ESA and the PI instrument teams who have contributed towards making XMM-Newton an outstanding success. The support of PPARC, CEA and ESA in funding large parts of the post-launch calibration activities is gratefully acknowledged.

## REFERENCES

1. F. Jansen et al., \XMM-Newton Observatory," A & A 365, p. L1, 2001.
2. M. J. L. Turner et al., \The European Photon Imaging Camera on XMM-Newton: The MOS cameras," A & A 365, p. L27, 2001.
3. L. Struder et al., \The European Photon Imaging Camera on XMM-Newton: The pn-ccd camera," A & A 365, p. L18, 2001.
4. A. Holland, \The effect of bulk traps in proton irradiated EEV ccds," NIM A 326, p. 335, 1993.
5. P. Ferrando et al., \Status of the EPIC/MOS calibration onboard XMM-Newton," Proc. SPIE 4851, p. 232, 2003.
6. A. Holland, A. Abbey, D. Lumb, and K. McCarthy, \Proton damage effects in EEV charge coupled devices," Proc. SPIE 1344, p. 378, 1990.
7. G. Y. Prigozhin et al., \Radiation damage in the Chandra x-ray CCDs," Proc. SPIE 4012, p. 720, 2000.
8. A. Abbey et al., \The Effect of Low Energy Protons on the Operational Characteristics of EPIC-MOS CCDs," Proc. RADECS, 2001.
9. B. Altieri, \Estimate of EPIC soft-proton dose in 3 years of mission," XMM-SOC-CAL-TN-0035, 2003.
10. E. Kendziorra et al., \The effect of low energy protons on the performance of the EPIC pn-CCD detector on XMM-Newton," Proc. SPIE 4140, p. 32, 2000.
11. J. W. den Herder, \The Reflection Grating Spectrometer on XMM-Newton," A & A 365, p. L7, 2001.
12. P. Dhez, \Institut d'Astrophysique Spatiale (IAS) 0.1- to 15-keV synchrotron radiation facility beam lines," Proc. SPIE 3144, p. 134, 1997.
13. A. D. Short, A. Keay, and M. J. L. Turner, \Performance of the EPIC MOS CCD detectors," Proc. SPIE 3445, p. 13, 1998.
14. J. Hiraga et al., \Direct measurement of sub-pixel structure of the EPIC MOS CCD on-board the XMM/Newton satellite," Nucl. Instr. and Meth. A 465, p. 384, 2001.
15. S. M. Kahn et al., \High resolution X-ray spectroscopy of I Zw 18 with the XMM-Newton reflection grating spectrometer," A & A 365, p. L312, 2001.
16. C. P. de Vries, J. Vink, M. Mendez, and F. Verbunt, \Long-term variability in the X-ray emission of RX J0720.4-3125," A & A 415, p. 31, 2004.